

Fundamental physics using the temporal gravitational wave background

Suvodip Mukherjee¹, Joseph Silk^{2,3,4}

¹*Gravitation Astroparticle Physics Amsterdam (GRAPPA), Anton Pannekoek Institute for Astronomy and Institute for High-Energy Physics, University of Amsterdam, Science Park 904, 1090 GL Amsterdam, The Netherlands*

²*Institut d'Astrophysique de Paris (IAP), UMR 7095, CNRS/UPMC Université Paris 6, Sorbonne Universités, 98 bis boulevard Arago, F-75014 Paris, France*

³*The Johns Hopkins University, Department of Physics & Astronomy, Bloomberg Center for Physics and Astronomy, Room 366, 3400 N. Charles Street, Baltimore, MD 21218, USA*

⁴*Beecroft Institute for Cosmology and Particle Astrophysics, University of Oxford, Keble Road, Oxford OX1 3RH, UK*

We propose a novel probe of fundamental physics by the exploitation of the temporal correlations between the multi-frequency electromagnetic (EM) signal and the stochastic gravitational wave background (SGWB) ¹⁻⁷ originating from coalescing binaries. This method will be useful for the detection of EM counterparts associated with SGWB sources. Measurement of the inevitable time-domain correlations between different frequencies of gravitational and EM waves ⁸⁻¹⁶ will test several aspects of fundamental physics and theory of gravity, and explore a new pathway for studying the universal nature of binary compact objects up to high

redshifts. Exploiting the time delay between concomitant emission of the gravitational wave and EM signals enables inference of the redshifts of the contributing sources by studying the time delay dilation due to cosmological expansion, if the time-lag between the emission of gravitational wave signal and EM signal acts like a standard clock. Exploration of the time-domain correlations between multi-messenger probes will bring new research directions to the understanding of transient sources, in a way that is accessible with current and future gravitational wave observatories¹⁷⁻²³.

Multi-frequency observations of a coalescing binary object in both gravitational and electromagnetic (EM) waves were first made for the neutron star binary merger GW170817²⁴⁻²⁷. This event left its imprint in the gravitational wave signal, as well as on the EM signals from gamma rays to the radio domain. Such an event makes it possible to study both astrophysical and cosmological aspects²⁷⁻³⁰. Analogously to this relatively nearby event, there inevitably are multiple astrophysical sources (binary neutron stars (BNSs), neutron star-black hole (NS-BHs), and binary black holes (BBHs)) coalescing in the observational Universe at high redshifts that cannot be detected as individual events. However distant events contribute to, and even dominate, the energy density of the stochastic gravitational wave background (SGWB). This is expressible, with respect to the critical energy density of the Universe $\rho_c c^2 = 3H_0^2 c^2 / 8\pi G$, and the number of compact objects $n(z, t_r(z), \theta, \hat{\alpha})$ coalescing in direction $\hat{\alpha}$ emitting gravitational wave signal per comoving volume between time $t_r(z)$ to $t_r(z + \Delta z)$ for the astrophysical parameters denoted by $\theta \in \{\text{mass}$

of the coalescing binaries, spin, inclination angle} with probability $p(\theta)$ ¹⁻⁷, as

$$\Omega_{GW}(f, t, \hat{\alpha}) = \frac{1}{\rho_c c^2} \int dz \int d\theta p(\theta) \frac{n(z, t_r(z), \theta, \hat{\alpha})}{(1+z)} \frac{dE_{GW}}{d \ln f_r}(f_r, \theta, t_r(z), \hat{\alpha}) \Big|_{f_r=(1+z)f}, \quad (1)$$

where $t_r(z)$ is the time in the source frame and t is the time in the observer's frame and the observed frequency which is related to the source frequency by the relation $f = f_r/(1+z)$. The number of overlapping coalescing binaries which contribute to the SGWB signal in a particular time t at a frequency f can be determined using the duty cycle (see Methods section) which is shown in Fig. 1 for the merger rates $\dot{n}_{BBH} = 100 \text{ Gpc}^{-3} \text{ yr}^{-1}$, $\dot{n}_{NS-BH} = 30 \text{ Gpc}^{-3} \text{ yr}^{-1}$, and $\dot{n}_{BNS} = 10^3 \text{ Gpc}^{-3} \text{ yr}^{-1}$ ^{31,32}. The duty cycle for stellar origin compact objects is going to be less than one for SGWB frequency $f > 20 \text{ Hz}$, and as a result, the sources contributing to the SGWB are non-overlapping and can be distinguished. The difference in the duty cycle is going to show different temporal behaviors of the SGWB signal for different kinds of compact objects (such as BNSs, NS-BHs, and BBHs), that can be used to differentiate between these sources⁷. The current upper bounds on the all sky-integrated strength of SGWB and directional SGWB from the O1+O2 data of LIGO-Hanford, LIGO-Livingston, and Virgo is 4.8×10^{-8} ⁵ and 14×10^{-8} (using the broad band radiometry method)⁶ respectively for $\Omega_{GW}(f) \propto f^{2/3}$. The strength of the SGWB power spectrum is a direct probe to the merger rate of the high redshift sources^{7,33,34} and can also be used for estimation of the event rate of lensed systems³⁵.

The astrophysical gravitational wave sources which are also likely to emit EM signals include BNS⁸⁻¹⁰, NS-BH¹¹, BBHs^{36,37}, and supermassive BBHs (SMBHs)¹¹⁻¹⁶. The characteristic time-delay in the source frame between emission in the rest frame $\Delta t_{f_r, \nu_r}$ is associated with the binary system properties, and unlikely to depend on source redshift. These sources can emit EM signals

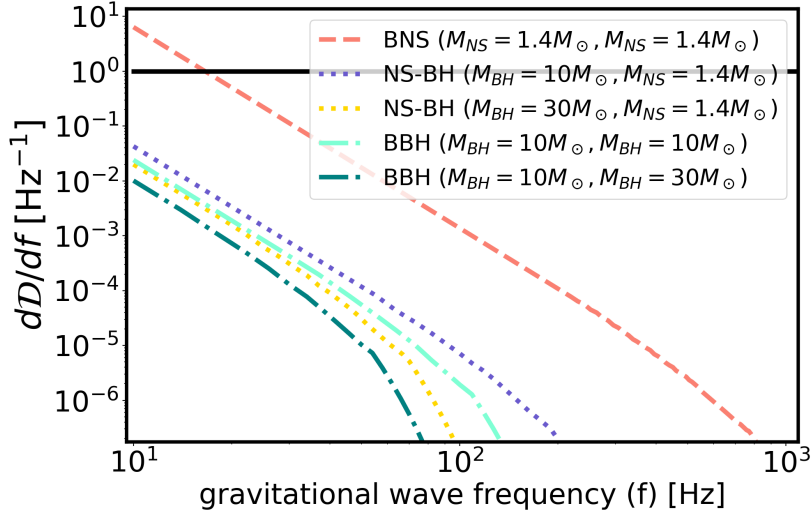


Figure 1: We show the duty cycle as a function of frequency for BNS, NS-BHs and BBHs in the frequency range observable from the ground based gravitational wave detectors. For non-overlapping gravitational wave sources, the values of the duty cycle are less than one.

over a wide range of frequencies ranging from gamma-rays to radio signals. The corresponding intensity of the EM signal from all the sources $\mathcal{I}(\nu, t, \hat{\alpha})$ can be expressed as

$$\mathcal{I}_\nu(t, \hat{\alpha}) = \int dz \frac{c}{4\pi H(z)(1+z)^3} \int d\theta p(\theta) n(z, t_r(z), \theta, \hat{\alpha}) L_{EM}(\nu_r, \theta, t_r(z), z, \hat{\alpha}) \Big|_{\nu_r=(1+z)\nu}, \quad (2)$$

where $L_{EM}(\nu_r, \theta, t_r(z), z, \hat{\alpha})$ is the luminosity of the EM signal at the source frequency $\nu_r = (1+z)\nu$ from a binary system with intrinsic source parameters denoted by $\theta \in \{\text{mass of the coalescing binaries, spin, inclination angle}\}$ at the time in the source frame $t_r(z)$ from sky direction $\hat{\alpha}$. The luminosity of the EM signal $L_{EM}(\nu_r)$ depends on the properties of the astrophysical systems and on the stage of the merger^{8–10}, but the true nature of $L_{EM}(\nu)$ for different sources is not yet known from observations. The characteristic properties of the light curves at different EM frequency bands are likely to be different for BNS^{8–10}, NS-BH¹¹, and SMBHs^{11–16}. The behavior of the EM signal

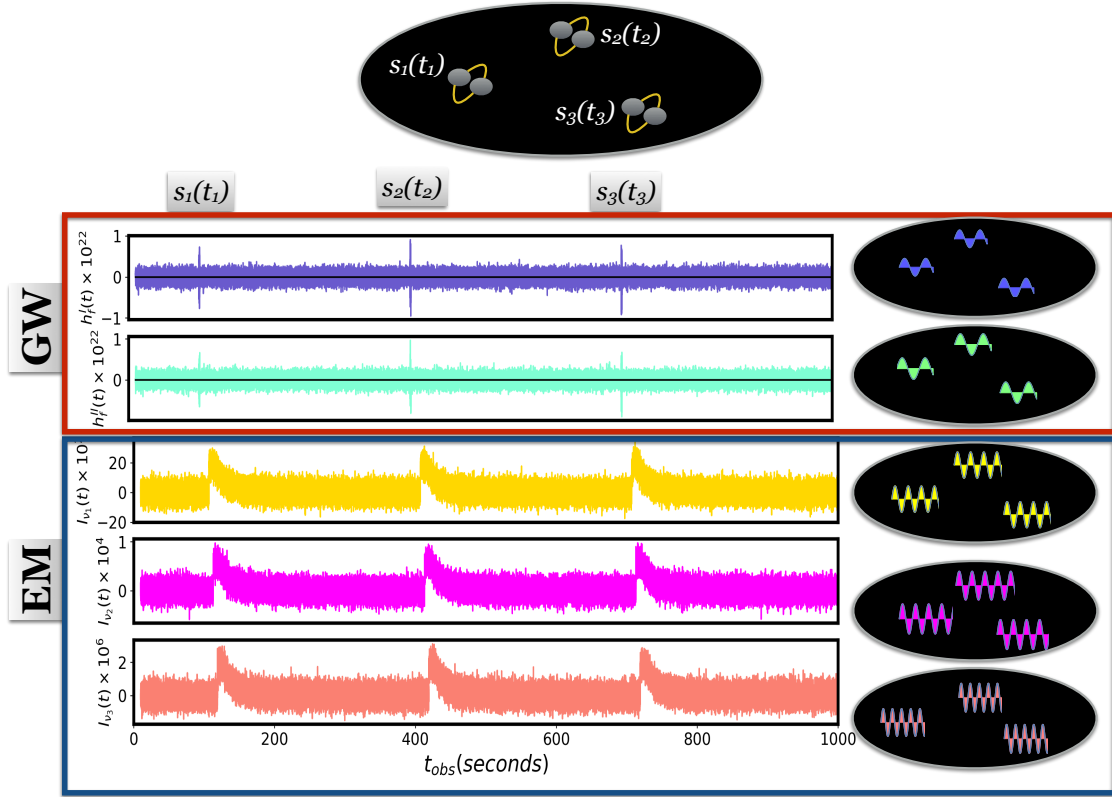


Figure 2: A schematic diagram showing the basic principle behind the time-domain correlation between SGWB and EM signal from the same sky location. In the upper panel we show the simulated time-series data at a gravitational wave frequency f for two different detector setup denoted by I and II . The three exaggerated gravitational wave signals $s(t_i)$ are shown at time t_i for the purpose of illustration assuming three different sky location shown by the map in the right. In the bottom panel, we show the simulated time-series data of the EM signals $s(t_i + \Delta t)$ from these sources after time Δt at three different EM frequencies ν_1, ν_2, ν_3 . The corresponding sky map of the EM signal is shown in the right for three different frequency channels. For the purpose of the illustration, we have considered a simple case of emission of the EM signal after a same time difference Δt in all the frequency channels.

and their light curve properties can be used to differentiate between different types of sources and their morphology.

The emission of the EM signals at frequency ν from gravitational wave sources emitting at frequency f (during inspiral, or merger, or ringdown phase) will lead to an inevitable correlation in the time domain with a time-lag $\Delta t_{f\nu} = t_f - t_\nu$ at fixed sky direction. A schematic diagram is shown in Fig. 2 explaining the underlying principle of the temporal correlation. Gravitational wave sources contributing to the SGWB can be detected in two different detectors denoted as h_I and h_{II} at an observed frequency f (shown in the upper two panels). If the binary source emitting the gravitational wave signal also emits an EM signal at different frequencies ν_1, ν_2 , and ν_3 (three lower panels) after a time delay $\Delta t_{f\nu_i}$, then it will appear in the same sky location.

The expected time-domain correlation function can be written as

$$C_{f\nu}(t_{obs}, \Delta t_{f\nu}, \hat{\alpha}) = \int \frac{dz}{4\pi\rho_c c H(z)(1+z)^4} \int d\theta p(\theta) n^2(z, t_r(z), \theta, \hat{\alpha}) \frac{dE_{GW}}{d \ln f_r}(f_r, \theta, t_{f_r}(z), \hat{\alpha}) \\ \times L_{EM}(\nu_r, \theta, t_{\nu_r}(z), \hat{\alpha}) \delta(t_{f_r}(z) - t_{\nu_r}(z) - \Delta t_{f_r\nu_r}(z)), \quad (3)$$

where, $\Delta t_{f_r\nu_r} = \Delta t_{f\nu}/(1+z)$ is relation between the correlation time-scale between the source frame and the observer frame, and t_{f_r} (and t_{ν_r}) are the time in the source frame for the SGWB signal (and EM signal). If a gravitational wave source contributing to the SGWB has follow-up EM emission after a time delay $\Delta t_{f_r\nu_r}$ after the end of the inspiral stage of the binary in its rest frame, then assuming the general theory of relativity, the observed time delay is

$$\Delta t_{f_{obs}\nu} = \int_{f_{obs}}^{f_{merg}} \frac{d\tau}{df} df + (1+z)\Delta t_{f_r\nu_r}, \quad (4)$$

where the first term denotes the duration of the gravitational wave signal between the observed frequency f_{obs} and the frequency at the end of the inspiral phase f_{merg} in the observer's frame, after which the EM emission at frequency ν_r can be characterised by the time duration $\Delta t_{f_r\nu_r}$. Since from the SGWB, we cannot measure the phase of the gravitational wave signal, we cannot infer the stage of the inspiraling binary system which we observe at frequency f_{obs} . As a result, the first term is an unknown shift for every pair of combinations of f_r and ν_r . However as this time-shift is constant for multiple frequency bands of the EM signal, we can exploit the characteristic time-lag between gravitational wave signal and EM signal at two different frequencies ν and ν' for a same SGWB signal by

$$\Delta t_{f_{obs}\nu\nu'} \equiv \Delta t_{f_{obs}\nu} - \Delta t_{f_{obs}\nu'} = (1+z)\Delta t_{f_r\nu_r\nu'_r}, \quad (5)$$

where $\Delta t_{f_r\nu_r\nu'_r} \equiv \Delta t_{f_r\nu_r} - \Delta t_{f_r\nu'_r}$ is the difference between the characteristic time-scale for gravitational wave emission at frequency f_r and EM emission at frequencies ν_r and ν'_r in the source rest frame. The characteristic time-scale $\Delta t_{f_r\nu_r\nu'_r}$ is related to the underlying physical mechanism associated with the astrophysical systems, and will not depend on the observation time and sky direction ¹. If the characteristic time-scale $\Delta t_{f_r\nu_r\nu'_r}$ is driven primarily by the scales associated with the astrophysical compact objects, then it is unlikely to depend on the cosmic epoch and its source redshift z . As a result, we can expect the characteristic time-scale to be unique and act like a *standard clock* for similar kinds of binary systems. The time difference $\Delta t_{f_r\nu_r\nu'_r}$ in the rest frame of the source is going to vary for different types of binaries (BNS, NS-BH, BBHs, SMBHs), but can be characterised as standard clock for each individual types of binaries. By using the EM spec-

¹Arising from the fact that the Universe is isotropic

trum \mathcal{I}_ν , we can characterize the type of sources contributing to the SGWB and the characteristic time-scale $\Delta t_{f_r\nu_r\nu'_r}$ can be modelled from the low redshift individual events.

Using such a standard clock, we can infer the source redshift using Eq. (5). The corresponding minimum variance estimator for inferring the redshifts of the gravitational wave sources by combining all N frequency channels is

$$1 + \hat{z} = \left(\sum_N \frac{1}{2\sigma_{t_{GW}}^2(f) + \sigma_{t_{EM}}^2(\nu) + \sigma_{t_{EM}}^2(\nu')} \right)^{-1} \sum_N \frac{1}{2\sigma_{t_{GW}}^2(f) + \sigma_{t_{EM}}^2(\nu) + \sigma_{t_{EM}}^2(\nu')} \frac{\Delta t_{f\nu\nu'}}{\Delta t_{f_r\nu_r\nu'_r}}, \quad (6)$$

where $\sigma_{t_{GW}}^2(f)$ and $\sigma_{t_{EM}}^2(\nu)$ are the measurement errors associated with the arrival time of the gravitational wave and EM wave. The variance σ_z^2 on inferred redshift \hat{z} is $\sigma_z^2 = \left(\sum_N \frac{1}{2\sigma_{t_{GW}}^2(f) + \sigma_{t_{EM}}^2(\nu) + \sigma_{t_{EM}}^2(\nu')} \right)^{-1}$.

For about a kHz sampling rate of the gravitational wave signal and EM signal, we can measure the redshift by this avenue with an accuracy $\sigma_z \sim 10^{-3}$ from a single combination of the frequency channels f , ν and ν' . A further reduction in the error bar (by $1/\sqrt{N}$) is possible by combining all the channels. An alternative way to find the redshift of the SGWB sources can be through identifying the host galaxy from an photometric/spectroscopic follow up using EM telescopes^{38–45} after observing the EM counterparts for those signals which shows a strong time-domain correlation with the GW signal.

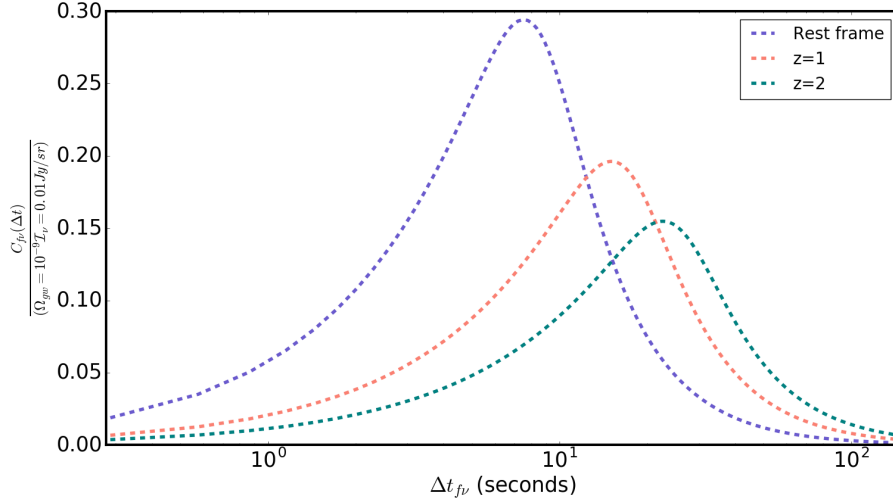


Figure 3: We show the correlation as the function of the time delay $\Delta t_{f\nu}$ between the SGWB signal at frequency f and EM signal at frequency ν from two different cosmological redshift $z = 1$, and $z = 2$. For comparison we show the expected correlation in the rest frame.

By estimation of the redshift from the standard clock method (given in Eq. 6) or by the host galaxy identification, we can write Eq. (3) as a tomographic estimate at every redshift (see Eq. (5)). After integrating over the observation time and sky directions, we can obtain the time-domain correlation signal as ²

$$C_{f\nu}(\Delta t_{f\nu} = \Delta t_{f_r\nu_r}(1+z)) = \int \frac{d\theta p(\theta)n^2(z, t_{f_r}, \theta)}{\rho_c c H(z)(1+z)^4} \times \left\langle \frac{dE_{GW}}{d \ln f_r}(f_r, \theta, t_{f_r}(z)) L_{EM}(\nu_r, \theta, t_{f_r}(z) + \Delta t_{f_r\nu_r}(z), z) \right\rangle_{t_{obs}, \hat{\alpha}}. \quad (7)$$

This signal depends on the intrinsic source property of the astrophysical system (the term present in the angular bracket), number density of emitting systems $n(z, t', \theta)$, and the expansion history of the Universe $H(z)$. The spectral shape of the time-domain correlation signal depends on the

²The angular bracket $\langle \cdot \rangle_{t_{obs}, \hat{\alpha}} \equiv \frac{1}{T_{obs} 4\pi} \int d^2\hat{\alpha} \int dt$

spectral shape of the EM signal L_{EM} . Even in the absence of a characteristic time-scale $\Delta t_{f\nu}$, the time-domain cross-correlation signal between gravitational waves and EM signal will exist, and can be used to explore the property of the astrophysical sources.

The expected correlation between SGWB signal and a power-law model of the EM signal (see Eq. 14 in methods) is shown in Fig. 3 for sources at redshift $z = 1$ and $z = 2$. For comparison, we also plot the expected signal in the rest frame of the source. The shift and stretch in the curve happen due to time dilation arising from the expansion of the Universe. The behaviour of the temporal correlation function is going to be useful to study astrophysical systems such as BNSs, NS-BHs, SMBHs up to high redshift with the aid of the SGWB. For the correct association of the EM signal with the SGWB signal, it is required that the observed characteristic time-scale $\Delta t_{f\nu}$ between gravitational wave frequency f and EM frequency ν is shorter than the time gap between the emission of two signals Δt_{GW} at the same sky location in the SGWB map, i.e. $\Delta t_{f\nu} < \Delta t_{GW}$. Δt_{GW} is related to the event rate by the relation $\Delta t_{GW} = \left(\int \frac{dz c d_c^2 \dot{n}(z)}{H(z)(1+z)} \right)^{-1}$, where d_c denotes the comoving distance to redshift z .

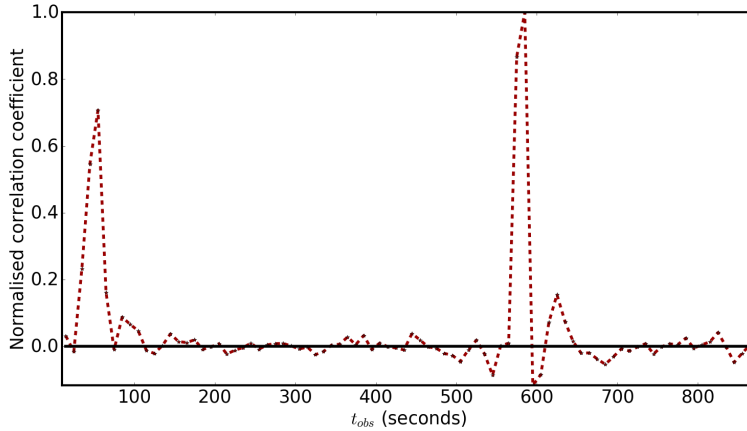


Figure 4: We show the normalised correlation coefficient between the mock time-series data of SGWB and EM signal as the function of the observation time t_{obs} after performing 10 seconds bin average. The correlation between the two are large when the signals are present in both the data samples (SGWB and EM signal), otherwise it does not show strong correlation.

To show a proof of principle of the time domain correlation, we implement this method on a simulated time-series data assuming two detectors ($h_I(t)$ and $h_J(t)$) and EM signals $\mathcal{I}_\nu(t)$ for two frequency channels. The simulated time-series is assumed to have two injected sub-threshold gravitational wave signal at the level $0.5\text{-}\sigma_{GW}$ (where σ_{GW} is the standard deviation of the gravitational wave detector noise) and the EM signal is considered to be 2σ above the noise background (see method section for the details). The time-domain cross-correlation between $\Omega_{GW}(f, t)$ and $\mathcal{I}_\nu(t)$ is shown in Fig. 4 after averaging over temporal window 10 seconds using the estimator given in Methods (see Eq. 15). The correlation between the two is large only when the signal is present in both SGWB mock data $\Omega_{GW}(f, t)$ and EM mock data $\mathcal{I}_\nu(t)$, otherwise, it shows no distinct feature in the cross-correlation. The time-domain correlation is going to be useful for searching for EM counterparts associated with the sources contributing to the SGWB. In the absence of the signal,

the cross-correlation between the two time-series does not lead to a constructive signal. This is the key aspect which makes the time-domain correlation between the gravitational waves and EM waves a clean way to measure the EM counterparts to the signals which ordinarily are hidden in the noise of the gravitational wave detector. Since EM detector noise having zero mean and is uncorrelated with the gravitational wave detector noise, makes it possible to find strong correlation only when the signal is present in both the EM and SGWB data. By combining the time-domain correlated measurement from multiple frequency bands of EM observations and exploiting their light-curve properties, one can identify the EM counterparts associated with the integrated SGWB.

Considering N_p number of sky patches with joint gravitational wave and EM signals detected all over the sky per year after combining all gravitational wave detectors, we can write the signal-to-noise ratio (SNR) for the measurement of the $C_{f\nu}(\Delta t_{f\nu})$ as

$$SNR(C_{f\nu}(\Delta t_{f\nu})) = \left(\sum_{T_{obs}} \left(\frac{N_p T_{obs}}{\text{yr}} \right) \frac{C_{f\nu}^2(\Delta t_{f\nu})}{\Delta\Omega_{N_{eff}}^2(f) \Delta\mathcal{I}_{N_{eff}}^2(\nu)} \right)^{1/2}, \quad (8)$$

where, $\Omega_{N_{eff}}^2(f)$ is the effective noise on the SGWB from all pairs of detectors at the gravitational wave frequencies f within the bandwidth Δf . $\Delta\mathcal{I}_{N_{eff}}^2(\nu)$ is the effective noise on the intensity of the EM signal at the frequency ν after combining all the detectors. The detailed estimation of the SNR for a network of gravitational wave detectors is discussed in the Methods section (see Eq. 16). Though, the high SNR SGWB measurement is going to be limited by the angular resolution $\Delta\Theta \sim 1$ radian⁷, EM counterpart measurements are going to provide accurate identification of sky localization. As a result, angular scales which are unresolved in the SGWB signal, can be probed with the aid of EM signals. Hence the number of independent sky patches N_p in the time-domain cross-correlation technique is going to be large and will be limited by the resolution of the

instruments measuring EM signal.

This new unexplored avenue proposed in this work makes it possible to study a broad range of scientific aspects in the field of astrophysics, cosmology, and fundamental physics. **Astrophysics:** (i) This method enables to search for the EM counterpart for the SGWB sources. (ii) The magnitude and shape of the correlation signal for different characteristic time $\Delta t_{f\nu}$ will explore the energy budget of the astrophysical sources and their temporal evolution up to high redshift. (iii) The time-domain correlation between the SGWB and EM signals will help to distinguish BNS and NS-BH systems from the BBHs (or sources without EM counterparts). (iv) The inference of the redshift of the source and the accurate sky localization of the gravitational wave sources from any EM counterparts is going to help in identifying the host galaxy. Hence the population of the gravitational wave host can be studied up to high redshift. (v) The redshift distribution of the merger rates can also be probed by this method which is going to be useful for distinguishing astrophysical compact objects and primordial black holes if the latter constitutes the dark matter.

Cosmology and Fundamental physics: (i) In the presence of a characteristic time-scale, the measurement of the time-dilation will provide direct evidence of the expansion of the Universe and can be used to identify the redshift to the sources contributing in SGWB using Eq. (6), (ii) The observed time delay between the gravitational wave and the EM signals makes it possible to study the speed of propagation of both signals in space-time. The constraints on the difference between the speed of propagation of gravitational waves c_{GW} and EM waves c_{EM} as $\Delta c_{EM-GW}/c_{EM} = c_{EM}\Delta t_{f\nu}/D_l(z)$ are going to improve by several orders of magnitude (by a

factor ($26 \text{ Mpc}/D_l(z)$) than the existing bounds from GW170817 ^{25,27}, due to the large luminosity distance $D_l(z)$ accessible to the SGWB sources. For example, sources contributing to the SGWB signal from redshift $z = 5$ are going to provide stronger constraints by a factor $\sim 10^4$ than the existing bound from GW170817 ^{25,27}. Moreover, all-sky averaging is going to reduce the uncertainties associated with the individual sources and will also improve the constraints by $\sqrt{N_p T_{obs}}$.

(iii) The dispersion of gravitational waves $E^2 = p^2 c^2 + m^2 c^4$ for different frequencies can be tested by comparing the time differences between the propagation of the gravitational wave signal and the EM signal $\Delta t_{f\nu}$. (iv) The comparison of the time delay for different frequencies is going to test the theory of gravity from the equivalence of the Shapiro time delay between gravitational wave signal and EM signal due to gravitational lensing ⁴⁶. Using the SGWB signal originating from different redshifts, a tomographic estimation of the Shapiro time delay can be measured. (v) With the availability of all-sky searches for the neutrino background ⁴⁷, the temporal cross-correlation between gravitational waves and neutrinos, and between EM signals and neutrinos can be explored.

The time-domain correlation between gravitational wave and EM signals will open a unique window to study the SGWB and its sources from the network of ongoing/upcoming detectors ⁴⁸ such as LIGO ^{17,49,50}, Virgo ^{18,51}, KAGRA ^{19,52}, LIGO-India ²⁰, and in the future from LISA ²¹, Cosmic Explorer ²², and Einstein Telescope ²³. Our proposed method will exploit the universal nature of the time-lag between the emission of the gravitational wave and EM signals (detectable from the ongoing/upcoming missions ^{38-45,53}), which can be used to determine the redshifts of the gravitational wave sources contributing to the SGWB. Using this method several aspects of astrophysics, cosmology, and fundamental physics are going to be explored. The time-domain

correlation proposed in this work applies also to the individual gravitational wave events, and also to the sub-threshold gravitational wave events. This will be explored in future work. Along with temporal correlation, the cross-correlation between EM and gravitational wave signal in the spatial domain is also going to provide a multi-messenger study of the Universe ^{54,55}. This new area of research using time-domain multi-messenger multi-frequency signals potentially develops a new domain for exploration of the cosmos at high redshift.

1. Allen, B. & Romano, J. D. Detecting a stochastic background of gravitational radiation: Signal processing strategies and sensitivities. *Phys. Rev. D* **59**, 102001 (1999). [gr-qc/9710117](#).
2. Phinney, E. S. A Practical theorem on gravitational wave backgrounds. *arXiv* (2001). [astro-ph/0108028](#).
3. Regimbau, T. & Chauvineau, B. Stochastic background from extra-galactic double neutron stars. *Class. Quant. Grav.* **24**, S627–S638 (2007). [0707.4327](#).
4. Zhu, X.-J., Howell, E., Regimbau, T., Blair, D. & Zhu, Z.-H. Stochastic Gravitational Wave Background from Coalescing Binary Black Holes. *Astrophys. J.* **739**, 86 (2011). [1104.3565](#).
5. Abbott, B. *et al.* Search for the isotropic stochastic background using data from Advanced LIGO’s second observing run. *Phys. Rev. D* **100**, 061101 (2019). [1903.02886](#).
6. Abbott, B. *et al.* Directional limits on persistent gravitational waves using data from Advanced LIGO’s first two observing runs. *Phys. Rev. D* **100**, 062001 (2019). [1903.08844](#).

7. Mukherjee, S. & Silk, J. Time dependence of the astrophysical stochastic gravitational wave background. *Monthly Notices of the Royal Astronomical Society* **491**, 4690–4701 (2019). URL <https://doi.org/10.1093/mnras/stz3226>. <https://academic.oup.com/mnras/article-pdf/491/4/4690/31570126/stz3226.pdf>.
8. Li, L.-X. & Paczynski, B. Transient events from neutron star mergers. *Astrophys. J. Lett.* **507**, L59 (1998). [astro-ph/9807272](https://arxiv.org/abs/astro-ph/9807272).
9. Metzger, B. D. & Berger, E. What is the Most Promising Electromagnetic Counterpart of a Neutron Star Binary Merger? *ApJ* **746**, 48 (2012). [1108.6056](https://arxiv.org/abs/1108.6056).
10. Barbieri, C., Salafia, O., Perego, A., Colpi, M. & Ghirlanda, G. Light-curve models of black hole – neutron star mergers: steps towards a multi-messenger parameter estimation. *Astron. Astrophys.* **625**, A152 (2019). [1903.04543](https://arxiv.org/abs/1903.04543).
11. Giacomazzo, B., Baker, J. G., Miller, M. C., Reynolds, C. S. & van Meter, J. R. General relativistic simulations of magnetized plasmas around merging supermassive black holes. *The Astrophysical Journal Letters* **752**, L15 (2012). URL <http://stacks.iop.org/2041-8205/752/i=1/a=L15>.
12. Haiman, Z. The X-ray Chirp of a Compact Black Hole Binary. *Found. Phys.* **48**, 1430–1445 (2018).
13. Palenzuela, C., Lehner, L. & Liebling, S. L. Dual Jets from Binary Black Holes. *Science* **329**, 927 (2010). [1005.1067](https://arxiv.org/abs/1005.1067).

14. Farris, B. D., Duffell, P., MacFadyen, A. I. & Haiman, Z. Binary Black Hole Accretion During Inspiral and Merger. *Mon. Not. Roy. Astron. Soc.* **447**, L80–L84 (2015). [1409.5124](#).
15. Gold, R. *et al.* Accretion disks around binary black holes of unequal mass: General relativistic MHD simulations of postdecoupling and merger. *Phys. Rev.* **D90**, 104030 (2014). [1410.1543](#).
16. Armitage, P. J. & Natarajan, P. Accretion during the merger of supermassive black holes. *Astrophys. J.* **567**, L9–L12 (2002). [astro-ph/0201318](#).
17. Abbott, B. P. *et al.* Sensitivity of the Advanced LIGO detectors at the beginning of gravitational wave astronomy. *Phys. Rev. D* **93**, 112004 (2016). [Addendum: *Phys.Rev.D* 97, 059901 (2018)], [1604.00439](#).
18. Acernese, F. *et al.* Advanced virgo: a second-generation interferometric gravitational wave detector. *Classical and Quantum Gravity* **32**, 024001 (2014). URL <https://doi.org/10.1088%2F0264-9381%2F32%2F2%2F024001>.
19. Akutsu, T. *et al.* KAGRA: 2.5 Generation Interferometric Gravitational Wave Detector. *Nat. Astron.* **3**, 35–40 (2019). [1811.08079](#).
20. Unnikrishnan, C. IndIGO and LIGO-India: Scope and plans for gravitational wave research and precision metrology in India. *Int. J. Mod. Phys. D* **22**, 1341010 (2013). [1510.06059](#).
21. Amaro-Seoane, P. *et al.* Laser Interferometer Space Antenna. *arXiv e-prints* arXiv:1702.00786 (2017). [1702.00786](#).

22. Reitze, D. *et al.* Cosmic Explorer: The U.S. Contribution to Gravitational-Wave Astronomy beyond LIGO. *Bull. Am. Astron. Soc.* **51**, 035 (2019). [1907.04833](#).
23. Punturo, M. *et al.* The Einstein Telescope: A third-generation gravitational wave observatory. *Class. Quant. Grav.* **27**, 194002 (2010).
24. Abbott, B. *et al.* Gravitational Waves and Gamma-rays from a Binary Neutron Star Merger: GW170817 and GRB 170817A. *Astrophys. J. Lett.* **848**, L13 (2017). [1710.05834](#).
25. Abbott, B. P. *et al.* Gw170817: Observation of gravitational waves from a binary neutron star inspiral. *Phys. Rev. Lett.* **119**, 161101 (2017). URL <https://link.aps.org/doi/10.1103/PhysRevLett.119.161101>.
26. Abbott, B. *et al.* Multi-messenger Observations of a Binary Neutron Star Merger. *Astrophys. J. Lett.* **848**, L12 (2017). [1710.05833](#).
27. Abbott, B. P. *et al.* A gravitational-wave standard siren measurement of the Hubble constant. *Nature* **551**, 85–88 (2017). [1710.05835](#).
28. Margutti, R. *et al.* The Electromagnetic Counterpart of the Binary Neutron Star Merger LIGO/VIRGO GW170817. V. Rising X-ray Emission from an Off-Axis Jet. *Astrophys. J. Lett.* **848**, L20 (2017). [1710.05431](#).
29. Cowperthwaite, P. *et al.* The Electromagnetic Counterpart of the Binary Neutron Star Merger LIGO/Virgo GW170817. II. UV, Optical, and Near-infrared Light Curves and Comparison to Kilonova Models. *Astrophys. J. Lett.* **848**, L17 (2017). [1710.05840](#).

30. Annala, E., Gorda, T., Kurkela, A. & Vuorinen, A. Gravitational-wave constraints on the neutron-star-matter equation of state. *Phys. Rev. Lett.* **120**, 172703 (2018). URL <https://link.aps.org/doi/10.1103/PhysRevLett.120.172703>.
31. Abbott, B. *et al.* GWTC-1: A Gravitational-Wave Transient Catalog of Compact Binary Mergers Observed by LIGO and Virgo during the First and Second Observing Runs. *Phys. Rev. X* **9**, 031040 (2019). [1811.12907](https://arxiv.org/abs/1811.12907).
32. Abbott, B. *et al.* GW190425: Observation of a Compact Binary Coalescence with Total Mass $\sim 3.4M_{\odot}$. *Astrophys. J. Lett.* **892**, L3 (2020). [2001.01761](https://arxiv.org/abs/2001.01761).
33. Boco, L. *et al.* Merging Rates of Compact Binaries in Galaxies: Perspectives for Gravitational Wave Detections (2019). [1907.06841](https://arxiv.org/abs/1907.06841).
34. Callister, T., Fishbach, M., Holz, D. & Farr, W. Shouts and Murmurs: Combining Individual Gravitational-Wave Sources with the Stochastic Background to Measure the History of Binary Black Hole Mergers (2020). [2003.12152](https://arxiv.org/abs/2003.12152).
35. Mukherjee, S., Broadhurst, T., Diego, J. M., Silk, J. & Smoot, G. F. Inferring the lensing rate of LIGO-Virgo sources from the stochastic gravitational wave background (2020). [2006.03064](https://arxiv.org/abs/2006.03064).
36. McKernan, B. *et al.* Ram-pressure stripping of a kicked Hill sphere: Prompt electromagnetic emission from the merger of stellar mass black holes in an AGN accretion disk. *Astrophys. J. Lett.* **884**, L50 (2019). [1907.03746](https://arxiv.org/abs/1907.03746).

37. Graham, M. J. *et al.* Candidate electromagnetic counterpart to the binary black hole merger gravitational-wave event s190521g. *Phys. Rev. Lett.* **124**, 251102 (2020). URL <https://link.aps.org/doi/10.1103/PhysRevLett.124.251102>.
38. LSST Science Collaboration *et al.* LSST Science Book, Version 2.0. *ArXiv e-prints* (2009). [0912.0201](https://arxiv.org/abs/0912.0201).
39. Green, J. *et al.* Wide-Field InfraRed Survey Telescope (WFIRST) Final Report. *arXiv e-prints* arXiv:1208.4012 (2012). [1208.4012](https://arxiv.org/abs/1208.4012).
40. Spergel, D. *et al.* WFIRST-2.4: What Every Astronomer Should Know. *arXiv e-prints* arXiv:1305.5425 (2013). [1305.5425](https://arxiv.org/abs/1305.5425).
41. Aghamousa, A. *et al.* The DESI Experiment Part I: Science, Targeting, and Survey Design (2016). [1611.00036](https://arxiv.org/abs/1611.00036).
42. Refregier, A. *et al.* Euclid Imaging Consortium Science Book. *ArXiv e-prints* (2010). [1001.0061](https://arxiv.org/abs/1001.0061).
43. Dore, O. *et al.* Science Impacts of the SPHEREx All-Sky Optical to Near-Infrared Spectral Survey II: Report of a Community Workshop on the Scientific Synergies Between the SPHEREx Survey and Other Astronomy Observatories. *arXiv* (2018). [1805.05489](https://arxiv.org/abs/1805.05489).
44. Dore, O. *et al.* WFIRST Science Investigation Team "Cosmology with the High Latitude Survey" Annual Report 2017. *ArXiv e-prints* (2018). [1804.03628](https://arxiv.org/abs/1804.03628).

45. Bellm, E. C. *et al.* The zwicky transient facility: System overview, performance, and first results. *Publications of the Astronomical Society of the Pacific* **131**, 018002 (2018). URL <https://doi.org/10.1088%2F1538-3873%2Faaecbe>.
46. Shapiro, I. I. Fourth test of general relativity. *Phys. Rev. Lett.* **13**, 789–791 (1964). URL <https://link.aps.org/doi/10.1103/PhysRevLett.13.789>.
47. Aartsen, M. *et al.* IceCube Search for Neutrinos Coincident with Compact Binary Mergers from LIGO-Virgo’s First Gravitational-Wave Transient Catalog (2020). [2004.02910](https://arxiv.org/abs/2004.02910).
48. Abbott, B. *et al.* Prospects for Observing and Localizing Gravitational-Wave Transients with Advanced LIGO, Advanced Virgo and KAGRA. *Living Rev. Rel.* **21**, 3 (2018). [1304.0670](https://arxiv.org/abs/1304.0670).
49. Aasi, J. *et al.* Advanced LIGO. *Class. Quant. Grav.* **32**, 074001 (2015). [1411.4547](https://arxiv.org/abs/1411.4547).
50. Tse, M. *et al.* Quantum-enhanced advanced ligo detectors in the era of gravitational-wave astronomy. *Phys. Rev. Lett.* **123**, 231107 (2019). URL <https://link.aps.org/doi/10.1103/PhysRevLett.123.231107>.
51. Acernese, F. *et al.* Increasing the astrophysical reach of the advanced virgo detector via the application of squeezed vacuum states of light. *Phys. Rev. Lett.* **123**, 231108 (2019). URL <https://link.aps.org/doi/10.1103/PhysRevLett.123.231108>.
52. Aso, Y. *et al.* Interferometer design of the kagra gravitational wave detector. *Phys. Rev. D* **88**, 043007 (2013). URL <https://link.aps.org/doi/10.1103/PhysRevD.88.043007>.

53. Stratta, G. *et al.* THESEUS: a key space mission concept for Multi-Messenger Astrophysics. *Adv. Space Res.* **62**, 662–682 (2018). [1712.08153](#).
54. Mukherjee, S., Wandelt, B. D. & Silk, J. Multimessenger tests of gravity with weakly lensed gravitational waves. *Phys. Rev. D* **101**, 103509 (2020). [1908.08950](#).
55. Mukherjee, S., Wandelt, B. D. & Silk, J. Probing the theory of gravity with gravitational lensing of gravitational waves and galaxy surveys. *Mon. Not. Roy. Astron. Soc.* **494**, 1956–1970 (2020). [1908.08951](#).
56. Ajith, P. *et al.* A Template bank for gravitational waveforms from coalescing binary black holes. I. Non-spinning binaries. *Phys. Rev.* **D77**, 104017 (2008). [Erratum: *Phys. Rev. D* **79**, 129901 (2009)], [0710.2335](#).
57. Wu, C., Mandic, V. & Regimbau, T. Accessibility of the Gravitational-Wave Background due to Binary Coalescences to Second and Third Generation Gravitational-Wave Detectors. *Phys. Rev.* **D85**, 104024 (2012). [1112.1898](#).
58. Rosado, P. A. Gravitational wave background from binary systems. *Phys. Rev.* **D84**, 084004 (2011). [1106.5795](#).
59. Mitra, S. *et al.* Gravitational wave radiometry: Mapping a stochastic gravitational wave background. *Phys. Rev.* **D77**, 042002 (2008). [0708.2728](#).
60. Thrane, E. *et al.* Probing the anisotropies of a stochastic gravitational-wave background using a network of ground-based laser interferometers. *Phys. Rev.* **D80**, 122002 (2009). [0910.0858](#).

61. Talukder, D., Mitra, S. & Bose, S. Multi-baseline gravitational wave radiometry. *Phys. Rev. D* **83**, 063002 (2011). [1012.4530](#).
62. Romano, J. D. & Cornish, N. J. Detection methods for stochastic gravitational-wave backgrounds: a unified treatment. *Living Rev. Rel.* **20**, 2 (2017). [1608.06889](#).
63. Beuermann, K. *et al.* Vlt observations of grb 990510 and its environment. *Astron. Astrophys.* **352**, L26 (1999). [astro-ph/9909043](#).
64. Troja, E. *et al.* A year in the life of GW 170817: the rise and fall of a structured jet from a binary neutron star merger. *Mon. Not. Roy. Astron. Soc.* **489**, 1919–1926 (2019). [1808.06617](#).
65. Flanagan, E. E. Sensitivity of the laser interferometer gravitational wave observatory to a stochastic background, and its dependence on the detector orientations. *Phys. Rev. D* **48**, 2389–2407 (1993). URL <https://link.aps.org/doi/10.1103/PhysRevD.48.2389>.
66. Christensen, N. Measuring the stochastic gravitational-radiation background with laser-interferometric antennas. *Phys. Rev. D* **46**, 5250–5266 (1992). URL <https://link.aps.org/doi/10.1103/PhysRevD.46.5250>.

Acknowledgements Authors are thankful to Sharan Banagiri for carefully reviewing the manuscript and making valuable suggestions during the LSC internal review. S. M. would like to thank Joseph Romano for insightful discussions on the work. S. M. acknowledges useful comments during LIGO working group presentation from Thomas Callister, Shivaraj Kandaswamy, Andrew Matas, and Sanjit Mitra. This analysis

was carried out at the Horizon cluster hosted by Institut d'Astrophysique de Paris. We thank Stephane Rouberol for smoothly running the Horizon cluster. SM is supported by the research program Innovational Research Incentives Scheme (Vernieuwingsimpuls), which is financed by the Netherlands Organization for Scientific Research through the NWO VIDI Grant No. 639.042.612-Nissanke. The computational work of SM is partially supported by the Labex ILP (reference ANR-10-LABX-63) part of the Idex SUPER, received financial state aid managed by the Agence Nationale de la Recherche, as part of the programme Investissements d'avenir under the reference ANR-11-IDEX-0004-02.

Competing Interests The authors declare that they have no competing financial interests.

Correspondence Correspondence and requests for materials should be addressed to SM. (email: mukherje@iap.fr, s.mukherjee@uva.nl), and JS. (email: joseph.silk@physics.ox.ac.uk).

Methods

1 Gravitational wave signal from coalescing binaries

The compact objects contribute to the SGWB signal in its inspiral, merger, and ring down phase.

The corresponding energy spectrum per logarithmic frequency bin is

$$\frac{dE_{GW}(\theta)}{df_r} = \frac{(G\pi)^{2/3} \mathcal{M}_c^{5/3}}{3} \mathcal{G}(f_r), \quad (9)$$

where $\mathcal{G}(f_r)$ captures the frequency dependence of the gravitational wave signal which can be modeled as ⁵⁶

$$\mathcal{G}(f_r) = \begin{cases} f_r^{-1/3} & \text{for } f_r < f_{merg}, \\ \frac{f_r^{2/3}}{f_{merg}} & \text{for } f_{merg} \leq f_r < f_{ring}, \\ \frac{1}{f_{merg} f_{ring}^{4/3}} \left(\frac{f_r}{1 + (\frac{f_r - f_{ring}}{f_w/2})^2} \right)^2 & \text{for } f_{ring} \leq f_r < f_{cut}, \end{cases} \quad (10)$$

where $f_x = c^3(a_1\eta^2 + a_2\eta + a_3)/\pi GM$ in terms of total mass $M = m_1 + m_2$ and symmetric mass ratio $\eta = m_1 m_2 / M^2$. The values of a_1, a_2 , and a_3 for different f_x are mentioned in table 1 ⁵⁶. For a given coalescing binaries of masses m_1 and m_2 , the binaries will be emitting gravitational waves in the inspiral part up to frequency f_{merg} , followed by the ringdown part up to frequency f_{ring} , and will stop emitting gravitational wave signal after f_{cut} . f_w denotes the width of the Lorentzian function ⁵⁶. The frequency of the emitted gravitational wave signal is inversely proportional to the total mass M of the coalescing binaries as shown in Eq. (10), resulting into a higher observed frequency from the ring down phase for lighter total masses than for the systems composed with heavier total mass.

The duty cycle for the gravitational wave sources contributing to the SGWB signal is defined as ^{57,58}

$$\frac{d\mathcal{D}}{df} = \int dz \dot{n}(z) \frac{d\tau_d}{df}, \quad (11)$$

where $\dot{n}(z)$ is the global event rate as a function of the cosmological redshift z and the duration gravitational wave signal spends at frequency f is

$$\frac{d\tau_d}{df} = \frac{5c^5}{96\pi^{8/3}G^{5/3}\mathcal{M}_z^{5/3}f^{11/3}}, \quad (12)$$

where, \mathcal{M}_z is the redshifted chirp mass of the gravitational wave sources. For values of the duty cycle $\frac{d\mathcal{D}}{df} > 1$, the observed SGWB is dominated by the overlapping gravitational wave sources. In the opposite limit, the SGWB is going to be sporadic.

2 Time domain correlation on simulated data

The time-domain correlation between the stochastic gravitational wave background (SGWB) and the EM signal for different frequency bands of gravitational waves and EM waves is shown from a sample of simulated data as a proof of principle. For the gravitational wave data, we obtain time-series data for a pair of gravitational wave detectors $i \in \{I, J\}$ as $h_i(t) = s(t) + n_i(t)$, where $h_i(t)$ is the total gravitational wave strain in the i^{th} detector, composed of the gravitational wave signal $s(t)$ and the Gaussian noise realizations $n_i(t, \hat{x})$ for the i^{th} detector with known noise power spectrum according to the design sensitivity of the LIGO-Virgo detectors ^{17,18}. The Gaussian noise realization for different detectors are uncorrelated. For the gravitational wave signal, we consider binary neutron star (BNSs) of individual mass $M_{NS} = 1.4 M_\odot$ with two signals within a time-series data of length 1000 seconds. For BNSs, with the currently known event rate from LVC ³¹,

the duty cycle is ongoing to be less than one for frequency range $f \geq 20$ Hz (as shown in Fig. 1), which makes the sources non-overlapping in time-domain. So, we consider two non overlapping sources contributing to the SGWB signal in a mock data length of 1000 seconds. We apply the cross-correlation between the two simulated SGWB data $h_I(t)$ and $h_J(t)$, to obtain the SGWB power spectrum ($\hat{\Omega}_{GW}^{obs}(f, t, \hat{\alpha})$) at frequency f using ^{1,59-62}

$$\Omega_{IJ}^{obs}(f, t, \hat{\alpha}) \equiv \langle h_I(f, t) h_J^*(f', t) \rangle = \delta(f - f') \langle s_I(f, t, \hat{\alpha}) s_J^*(f', t, \hat{\alpha}) \rangle, \quad (13)$$

For the injected gravitational signals, we consider EM signal in the frequency bands $\nu_r = 10^7$ Hz and $\nu_r = 10^{13}$ Hz, with a simple model of the light-curve written in terms of the time duration $\Delta t_{f_r \nu_r}$ after the merger of the gravitational wave sources and emission of the EM signal in the source rest frame by ^{63,64}

$$I_{\nu_r}(\Delta t_{f_r \nu_r}) = A_{\nu} \left(\frac{\nu_r}{\nu_0} \right)^{-\beta} \left(\left(\frac{\Delta t_{f_r \nu_r}}{t_p} \right)^{-\alpha_1 \kappa} + \left(\frac{\Delta t_{f_r \nu_r}}{t_p} \right)^{\alpha_2 \kappa} \right)^{-1/\kappa}, \quad (14)$$

where for this simple model, t_p denotes the peak time whose value is taken as 9 seconds, the rise and the decay parameters α_1 and α_2 are taken as 0.9 and 2.0 respectively. The smoothness parameter $\kappa = 2$ is considered in this analysis. The frequency dependence of the emission is considered as a power-law with the index $\beta = 0.585$ with the pivot point $\nu_0 = 10^7$ Hz. The amplitude of the flux A_{ν} is considered to be frequency dependent with $A_{\nu=10^7 \text{ Hz}} = 0.01$ Jy/sr and $A_{\nu=10^{13} \text{ Hz}} = 10^{-3}$ Jy/sr. The standard deviation of the noise for the EM signal is considered to be constant in time as $\sigma_{I_{\nu}}/I_{\nu} = 0.5$ (which resembles only a 2σ detection of the EM signal).

Using the map of SGWB $\Omega_{GW}^{obs}(f, t, \hat{\alpha}) = \frac{(32\pi^3 f^3)}{3H_0^2} \delta(f - f') \langle h_I(f, t, \hat{\alpha}) h_J^*(f', t, \hat{\alpha}) \rangle$ ¹ at frequency f , we can write an estimator for the time-domain correlation with the intensity map

$\mathcal{I}^{obs}(\nu, t, \hat{\alpha})$ of the EM signal ³ as

$$\begin{aligned}
C_{f\nu}(t_{obs}, \Delta t_{f\nu}, \hat{\alpha}) &\equiv \left\langle \left(\Omega_{GW}^{obs}(f, t', \hat{\alpha}) - \Omega_{GW}^b(f, t') \right) \left(\mathcal{I}_\nu^{obs}(t' + \Delta t_{f\nu}, \hat{\alpha}) - \mathcal{I}_\nu^b(t' + \Delta t_{f\nu}) \right) \right\rangle, \\
&= \frac{1}{\delta t} \int_{t_{obs}-\delta t/2}^{t_{obs}+\delta t/2} dt' \left(\Omega_{GW}^{obs}(f, t', \hat{\alpha}) - \Omega_{GW}^b(f) \right) \left(\mathcal{I}_\nu^{obs}(t' + \Delta t_{f\nu}, \hat{\alpha}) - \mathcal{I}_\nu^b \right),
\end{aligned} \tag{15}$$

where, δt is the small time interval over which we average the signals between the EM signal at frequency ν , with the gravitational wave signal at frequency f . The averaging time is much larger than the sampling time step δt_{sam} of the SGWB signal, and small/similar to the temporal correlation scale $\Delta t_{f\nu} = (1+z)\Delta t_{f_r\nu_r}$, i.e. $\delta t_{sam} \ll \delta t \lesssim \Delta t_{f\nu}$. $\Omega_{GW}^b(f)$ and $\mathcal{I}_s^b(\nu)$ is the sky and time averaged background. In the absence of a correlated signal in both $\Omega_{GW}(f)$ and $\mathcal{I}_s^{obs}(\nu)$, the above estimator given in Eq. (15) vanishes. The cross-correlation technique makes it possible to isolate the signal from the noise, even when the signal is weak as the noise between different detectors are uncorrelated. This shows that time-domain cross-correlation is a clean way to identify the EM counterparts to the SGWB sources.

We apply the estimator given in Eq. (15) between the SGWB signal $\Omega_{IJ}^{obs}(f, t, \hat{\alpha})$ with the intensity of the EM signal $\mathcal{I}_\nu(t + \Delta t)$ for different values of the time Δt with the integration time scale $\delta\tau = 10$ seconds. The cross-correlation signal between the mock data samples is shown in Fig. 4, indicating that the cross-correlation shows a spike when the signal is present in both SGWB and EM signal. The SGWB signal does not correlate with the noise in the EM signal and shows correlation only with the astrophysical source at the same spatial location separated by time difference time $\Delta t_{f\nu}$.

³ $\mathcal{I}^{obs}(\nu, t, \hat{\alpha})$ is the EM signal within the resolved sky resolution of the SGWB.

3 Signal to noise ratio for network of gravitational wave detectors

The signal to noise ratio (SNR) for the measurement of the $C_{f\nu}(\Delta t_{f\nu})$ can be obtained by integrating over the observation time T_{obs} and all sky directions $\hat{\alpha}$. By estimating the SGWB signal over a frequency bandwidth Δf centered at f , and estimating the EM signal over a frequency bandwidth $\Delta\nu$, centered at ν , we can obtain the SNR as

$$SNR(C_{f\nu}(\Delta t_{f\nu})) = \left(\sum_k \sum_{ij, i>j} \sum_{T_{bins}} \sum_{N_{pix}} \int_{f'-\Delta f'/2}^{f'+\Delta f'/2} df \int_{\nu'-\Delta\nu'/2}^{\nu'+\Delta\nu'/2} d\nu \frac{C_{f\nu}^2(t_{obs}, \Delta t_{f\nu}, \hat{\alpha})}{\Delta\Omega_{N_{ij}}^2(f) \Delta\mathcal{I}_{N_k}^2(\nu)} \right)^{1/2}, \quad (16)$$

where summation over k denotes all the EM missions observing the sky at frequency ν with detector noise power spectrum $\Delta\mathcal{I}_{N_k}^2(\nu)$ (and assuming that the background intensity signal $\mathcal{I}_s^b(\nu)$ is stationary), the sum over $\{ij\}$ denotes different pair of gravitational wave detectors, $\Delta\Omega_{N_{ij}}^2(f) = 100\pi^4 P_i P_j f^6 / 9H_0^4 \gamma^2(f, t, \hat{\alpha})$ is the SGWB noise power spectrum at frequency f ¹ which can be written in terms of the noise power spectrum of the i^{th} gravitational wave detector P_i (and P_j for the j^{th} detector), and the normalized overlap reduction function $\gamma(\hat{\alpha}, f, t)$ depends on the detector response function^{65,66}. $T_{bins} = T_{obs}/\delta t$ is the number of independent temporal bins available over the observation time T_{obs} , and N_p is the number of independent sky patches in the overlapping observed sky area f_{sky} between the map of SGWB and sky map of EM signal. The angular resolution of the SGWB map is diffraction limited given by $\Delta\Theta_{gw} = c/2fD$ where D is the distance between a pair of gravitational wave detectors. The above mentioned SNR improves with more observation time, more number of gravitational wave detectors and EM detectors, better sky resolution, and larger fraction of observable sky area.

f_i	a_1 ($\times 10^{-1}$)	a_2 ($\times 10^{-2}$)	a_3 ($\times 10^{-2}$)
f_{merg}	2.9740	4.4810	9.5560
f_{ring}	5.9411	8.9794	19.111
f_{cut}	8.4845	12.848	27.299
f_w	5.0801	7.7515	2.2369

Table 1: We show the values of the parameters to obtain the frequency f_{merg} , f_{ring} , f_{cut} , and f_w denoted by the functional form $f_i = c^3(a_1\eta^2 + a_2\eta + a_3)/\pi GM$ ⁵⁶.